

Received February 8, 2020, accepted February 19, 2020, date of publication February 24, 2020, date of current version March 9, 2020.

Digital Object Identifier 10.1109/ACCESS.2020.2975830

Research on Resistance Enhancement Coefficient and Thermal Dissipation of Stator Strands in Huge Synchronous Generator

LIKUN WANG^{1,2}, (Member, IEEE), BAOQUAN KOU², (Member, IEEE), AND WEI CAI^{1,3}

¹College of Electrical and Electronic Engineering, Harbin University of Science and Technology, Harbin 150080, China

²School of Electrical Engineering and Automation, Harbin Institute of Technology, Harbin 150001, China

³School of Electrical Engineering, Southeast University, Nanjing 210096, China

Corresponding author: Likun Wang (wkhello@163.com)


This work was supported in part by the National Natural Science Foundation of China under Grant 51907042, in part by the University Nursing Program for Young Scholars with Creative Talents in Heilongjiang Province under Grant UNPYSCCT-2018212, in part by the Heilongjiang Science and Technology Achievement Conversion and Cultivation Project under Grant TSTAU-C2018002, in part by the China Postdoctoral Science Foundation under Grant 2018T110270 and Grant 2017M620109, in part by the Postdoctoral Foundation of Heilongjiang Province of China under Grant LBH-Z17041, and in part by the Fundamental Research Foundation for Universities of Heilongjiang Province under Grant LGYC2018JC028.

ABSTRACT For large generators, accurate assessment for the resistance enhancement coefficient (REC) and thermal dissipation is of great significance. With the development of design and manufacturing technology for large generators, the different cross section of the upper and lower strand becomes an effective method to reduce the heat losses. In current electromagnetism design, the eddy current analysis does not take the strand structures into account. In this paper, the REC of strands with special structures of a 150MW turbo-generator is derived by an analytic algorithm. Besides that, a mathematical model of the stator slot is established and the heat losses distribution and REC of strands are calculated by finite element method (FEM). On this basis, the stator REC and thermal dissipation of a 1000MW power turbo-generator are investigated with hollow and solid strands. The calculated results match the experimental data. All of these could provide an important theoretical basis and reference for the design of stator windings in high-power generators.

INDEX TERMS Thermal dissipation, eddy current, turbo-generators.

I. INTRODUCTION

For traditional high-power turbo-generators, double layer windings with lap coils are often adopted for the stators. The strands of the upper and lower layers usually use the same structure, which have the same number of strands and strand cross section area. In this traditional structure, due to the transverse leakage of the magnetic field, a clear difference in eddy current distribution between the upper and lower strands appears. This could lead to significant temperature gradients along the radial direction. Under long operation processes of the generator, being affected by the action of thermal stress, strands and insulation of the windings may lead to wear, which may cause short-circuit fault and other accidents. Hence, the winding structure should be optimized

The associate editor coordinating the review of this manuscript and approving it for publication was Kan Liu .

to reduce the eddy current losses and improve its distribution to reduce the temperature gradients in the stator slot.

With these factors considered, several special strand structures, such as the strands number and the cross section being different for the upper and lower windings are proposed and applied to the stator windings of large turbo-generators to make the eddy current tend uniform distribution.

A vertically placed strip winding which can limit inter-turn short-circuit fault current, ac resistance of a litz wire, and current sharing analysis of parallel strands have been researched [1]–[3]. Copper losses with form-wound windings, online measuring power factor in ac resistance spot welding, and different tapped windings for flux adjustment have been investigated [4]–[6]. To reduce the harmonic contents of the rotor winding, a “double-sine” wound rotor is proposed for the brushless doubly fed generator [7]. In order to reduce the copper losses at high frequency, some experts have proposed to use rectangular litz wires in form-wound

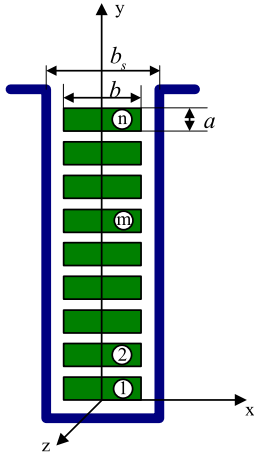


FIGURE 1. Stator winding with n strands in one slot.

stators [8], [9]. The proximity effect depends on the strength and frequency of magnetic field in the position where the conductor is located. Its impact on the copper losses is presented in [10]–[12]. For some complex structures, FEA could provide a desired solution [13]–[16]. Researchers have studied eddy current losses and ac resistance for the windings, but few do the research on REC of strands with special construction and thermal dissipation in large power turbo-generators. In this paper, a 150MW air-cooled turbo-generator is taken as an example. Eddy current losses of winding strands under rated load operation with special structures, where both the strands number and the cross section area are not the same, are derived by analytic algorithms. Based on the FEM, the physical and mathematical models of the stator slot are established with special strands structures. The magnetic field distribution of the slot is calculated. The real and imaginary currents are analyzed for each strand. The REC is obtained by real and imaginary currents. Comparing analytic and numerical algorithms, it can be shown that the deviation of REC gained by different algorithms is minor. Besides, the stator REC and thermal dissipation of a 1000MW power turbo-generator are investigated with hollow and solid windings. The heat sources of the hollow and solid windings are obtained and the RECs that are received from the magnetic field calculation are taken into account. The stator temperature is calculated based on a fluid and heat transfer principle [17]–[20]. The calculated temperature results and the test data are matched.

II. ANALYSIS FOR REC WITH DIFFERENT STRUCTURES

A. ANALYTIC AND NUMERICAL ALGORITHMS FOR REC WITH SAME STRANDS AREA

For an AC electrical machine, the stator current and leakage magnetic flux are alternating. Other than the load current, the eddy current could be induced in windings that are in the alternating magnetic field. The eddy current could lead the upper strands current density to increase, which results in a skin effect of the current. Both copper losses and effective resistance are increased [21]–[24].

A stator slot with n strands is shown in Fig. 1. The stator slot is an open rectangular slot. The current in each strand is $i = I_m \cos \omega t$. This is a sinusoidal magnetic field problem with two mediums. Some assumptions are listed as follows.

- (1) The stator slot in a large ac machine is usually deep and narrow. Thus, the leakage magnetic flux crossing the slot is parallel to the bottom. The circulating current effect is ignored.
- (2) The magnetic field intensity H_x is just the function of the coordinate y.
- (3) The stator core permeability is infinite and magnetic motive force drops is ignored.
- (4) The insulation matter has the same permeability as the vacuum. They are both $4\pi \times 10^{-7} \text{H/m}$. The relative permeability of the insulating material is 1. Besides that, the insulation material is non-conductive material, and its conductivity is 0. The insulation material itself does not be induced eddy current. The insulation matter does not change the distribution of the magnetic field in the slot.

Based on the assumption above, the magnetic flux that is generated by a winding with width b and current density J_z is equivalent to a magnetic flux that is generated by a winding with width b_s and current density bJ_z/b_s . Hence,

$$\begin{cases} \text{rot}H = k \frac{\partial H_x}{\partial y} = k \frac{b}{b_s} J_z \\ \text{rot}E = i \left(-\frac{\partial E_z}{\partial y} \right) = i (-j\omega B_x) \end{cases} \quad (1)$$

where H is magnetic field intensity, J_z is current density in z-direction, E is electric field intensity, and B_x is flux density in the x-direction. Only a one dimensional eddy equation should be solved as follows.

$$\frac{\partial^2 H_x}{\partial y^2} = j\omega \frac{b}{b_s} \mu_0 \sigma \dot{H}_x = p^2 \dot{H}_x \quad (2)$$

The solution for (2) is where

$$\dot{H}_x = A_1 e^{-py} + A_2 e^{py} \quad (3)$$

$$\begin{cases} p = \sqrt{j \frac{b}{b_s} \omega \mu_0 \sigma} = (1+j)k = \frac{1+j}{\Delta} \\ \Delta = \frac{1}{k} = \sqrt{\frac{b_s}{b} \cdot \frac{1}{\pi f \mu_0 \sigma}} \end{cases} \quad (4)$$

where Δ is the depth of penetration, A_1 and A_2 are arbitrary constants, which are determined by the boundary conditions. f is the frequency, μ_0 is the permeability of vacuum, and σ is the conductivity.

According to the law of ampere loop, there is

$$\dot{H}_x = \begin{cases} \frac{(m-1)}{b_s} I_m, & y = (m-1)a \\ \frac{m}{b_s} I_m, & y = ma \end{cases} \quad (5)$$

Hence, it could be expressed as follow.

$$\begin{cases} \frac{(m-1)}{b_s} I_m = A_1 e^{-p(m-1)a} + A_2 e^{p(m-1)a} \\ \frac{m}{b_s} I_m = A_1 e^{-pma} + A_2 e^{pma} \end{cases} \quad (6)$$

A_1 and A_2 can be gained, then the \dot{H}_x can be determined further.

$$\dot{H}_x = \frac{I_m}{2b_s} \frac{e^{pma}}{\sinh pa} (m-1 - me^{-pa})e^{-py} - \frac{I_m}{2b_s} \frac{e^{-pma}}{\sinh pa} (m-1 - me^{pa})e^{py} \quad (7)$$

For there is only one strand in a slot, the energy flow Π is in the y direction, so the plural power that flows in the slot conductor could be expressed by (8)

$$\begin{aligned} \int \Pi dS &= \frac{1}{2} b_s l [E_z H_{x(y=a)}^* - E_z H_{x(y=0)}] \\ &= \frac{1}{2} I_m^2 \frac{l}{\sigma b} \frac{p}{|\sinh pa|^2} \cosh pa \cdot \sinh p^* a \\ &= \frac{1}{2} I_m^2 \frac{l}{\sigma b \Delta} \left[\frac{\sinh 2\xi + \sin 2\xi}{\cosh 2\xi - \cos 2\xi} + j \frac{\sinh 2\xi - \sin 2\xi}{\cosh 2\xi - \cos 2\xi} \right] \end{aligned} \quad (8)$$

where $0 < \xi < 1$, $\xi = a/\Delta$, a is the height of strand, and l is the conductor length.

As there are n strands in one slot, the AC resistance of strand m could be expressed as

$$\begin{aligned} R_m &= \frac{b_s l}{I_m^2} \text{Re}[E_z H_{x(y=ma)}^* - E_z H_{x(y=(m-1)a)}] \\ &= \frac{l}{\sigma b_s} \text{Re} \left\{ \frac{p}{|\sinh pa|^2} [(2m^2 - 2m - 1) \cosh pa \cdot \sinh p^* a - 2m(m-1) \sinh p^* a] \right\} \\ &= \frac{1}{\sigma} \frac{l}{ba} \left[\xi \frac{\sinh 2\xi + \sin 2\xi}{\cosh 2\xi - \cos 2\xi} + m(m-1) 2\xi \frac{\sinh \xi - \sin \xi}{\cosh \xi + \cos \xi} \right] \end{aligned} \quad (9)$$

The REC of strand m k_{rm} can be obtained.

$$k_{rm} = \xi \frac{\sinh 2\xi + \sin 2\xi}{\cosh 2\xi - \cos 2\xi} + m(m-1) 2\xi \frac{\sinh \xi - \sin \xi}{\cosh \xi + \cos \xi} \quad (10)$$

where

$$\begin{cases} \varphi(\xi) = \xi \frac{\sinh 2\xi + \sin 2\xi}{\cosh 2\xi - \cos 2\xi} \\ \psi(\xi) = 2\xi \frac{\sinh \xi - \sin \xi}{\cosh \xi + \cos \xi} \end{cases} \quad (11)$$

Fig. 2 (a) gives the two function curves of equation (11). These two functions are both increasing function. It can be seen that $\varphi(\xi) \in [1, 5]$ and $\psi(\xi) \in [0, 10]$ for $\xi \in [0, 5]$.

In order to analyze the relationship of REC with the total number of strands in one slot, analytical and numerical calculations are conducted. Fig. 2 (b) shows the maximum REC with the total number of strands range from 1 to 28 when $b/b_s=0.8$ with analytical and numerical algorithms. The analytical and numerical algorithms match well. It can be seen that the maximum REC of the strand first increases with the increase of the total number of strands, and then decreases with the further increase of total number of strands. As the total number of strands is 3, the maximum REC of a strand is the maximum.

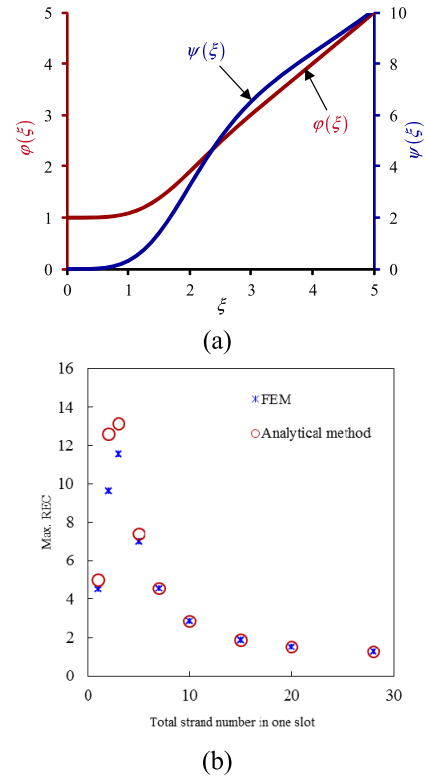


FIGURE 2. The function curves and max. REC. (a) Function curves of φ_ξ and ψ_ξ . (b) Max. REC with different total number of strands in one slot.

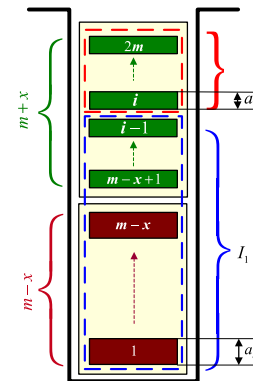


FIGURE 3. Slot structure with different number of strand and different cross section areas between the upper and lower windings.

B. ANALYTIC AND NUMERICAL ALGORITHMS FOR REC WITH SPECIAL STRAND CONSTRUCTION

Aiming at the different number and cross section area between the upper and lower winding strands, the REC of strands are derived by the following process. The structure of strands is shown in Fig. 3. The total number of upper strands is $m+x$, and lower strands is $m-x$.

In Fig. 3, $S_1 = S_2 = \dots = S_{m-x} > S_{m-x+1} = S_{m-x+2} = \dots = S_{2m}$, where S represent the strand area. The assumptions are the same as those in Section II A.

For the upper strand, the REC of strand i (k_{uri}) can be expressed as

$$k_{uri} = \varphi(\xi) + \frac{I_1^2 + I_1 I_i}{I_i^2} \psi(\xi) \quad (12)$$

where I_1 is the total current from strands 1 to $i-1$, and I_i is the current of strand i . The strand current could be expressed as

$$\begin{cases} i_i = i_c \frac{m}{m+x} \\ i_h = i_c \frac{m}{m-x} \end{cases} \quad (13)$$

where i_h is the current of the lower winding strand, and i_c is the strand current when the upper and lower strands have the same number and areas. Hence, it can be obtained that

$$\frac{I_1^2 + I_1 I_i}{I_i^2} = 2x(x-1) + 4xi + i^2 - i \quad (14)$$

The average REC of the upper winding (k_{urav}) can be expressed as

$$\begin{aligned} k_{urav} &= \frac{1}{m+x} \sum_{i=m-x+1}^{2m} K_{uri} \\ &= \varphi(\xi) + [2x(2x-1) + \frac{4x}{m+x} \sum_{i=m-x+1}^{2m} i \\ &\quad + \frac{1}{m+x} \sum_{i=m-x+1}^{2m} (i^2 - i)] \psi(\xi) \end{aligned} \quad (15)$$

As

$$\sum_{i=m-x+1}^{2m} i = \sum_{i=1}^{2m} i - \sum_{i=1}^{m-x} i \quad (16)$$

Hence, (16) can be further expressed as

$$\begin{aligned} k_{urav} &= 1 + 0.107 a_u^4 \left(\frac{b}{b_s}\right)^2 \left(\frac{f}{50}\right)^2 [3 \times 2x(3m+x) \\ &\quad + 6m(m-x) + (m+x)^2] \\ &= 1 + 7 \times 0.107 a_u^4 \left(\frac{b}{b_s}\right)^2 \left(\frac{f}{50}\right)^2 (m+x)^2 \end{aligned} \quad (17)$$

For further consolidation, (17) can be expressed as

$$k_{urav} = 1 + 7 \times 0.107 [(m+x)a_u]^2 \left(\frac{b \times a_u}{b_s}\right)^2 \left(\frac{f}{50}\right)^2 \quad (18)$$

where $(m+x)a_u$ is the total height of upper strands, $b \times a_u$ is upper the strand area, and a_u is the height of one upper strand.

For the lower winding, the derivation process for the average REC is the same as the upper winding. The average REC of the lower winding (k_{drav}) can be expressed as

$$k_{drav} = 1 + 0.107 [(m-x)a_d]^2 \left(\frac{b \times a_d}{b_s}\right)^2 \left(\frac{f}{50}\right)^2 \quad (19)$$

where $(m-x)a_d$ is the total height of lower strands, $b \times a_d$ is the lower strand area, and a_d is the height of one lower strand.

It can be seen that the winding average additional losses of the upper one is much greater than that of the lower one.

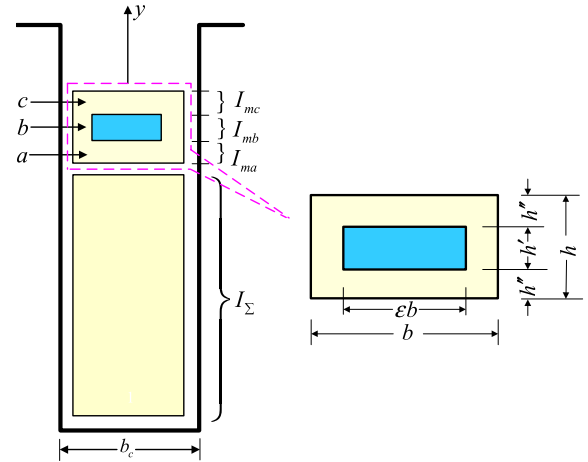


FIGURE 4. Slot structure with hollow strand.

The winding average additional losses of the upper one is seven times of that in the lower one when their total areas are the same. The average REC is direct proportion to the total height and strand area, and is inversely proportional to the slot width. The winding current is irrelevant.

For the hollow strand and the relations of structure size, which are shown in Fig.4, the REC of the hollow strand can also be derived by formulas (20)-(24).

$$\begin{cases} H_{xa} = \frac{1}{b_c \text{sh } p h''} [I_1 \text{sh } p y - I_{\Sigma} \text{sh } p(y-h'')] \\ E_{za} = \frac{p}{b \sigma \text{sh } p h''} [I_1 \text{ch } p y - I_{\Sigma} \text{ch } p(y-h'')] \end{cases} \quad (20)$$

$$\begin{cases} H_{xb} = \frac{1}{b_c \text{sh } p' h'} [I_2 \text{sh } p'(y-h') - I_1 \text{ch } p'(y-h'-h')] \\ E_{zb} = \frac{p'}{(1-\varepsilon)b \sigma \text{sh } p' h'} [I_2 \text{ch } p'(y-h') - I_1 \text{ch } p'(y-h'-h')] \end{cases} \quad (21)$$

$$\begin{cases} H_{xc} = \frac{(I_m + I_{\Sigma}) \text{sh } p(y-h''-h') - I_2 \text{sh } p(y-2h''-h')}{b_c \text{sh } p h''} \\ E_{zc} = \frac{p[(I_m + I_{\Sigma}) \text{ch } p(y-h''-h') - I_2 \text{ch } p(y-2h''-h')]}{b \sigma \text{sh } p h''} \end{cases} \quad (22)$$

where $I_1 = I_{ma} + I_{\Sigma}$, $I_2 = I_{ma} + I_{mb} + I_{\Sigma}$. I_{ma} , I_{mb} , and I_{mc} are the current of part a, b, and c, respectively. I_{Σ} is the current below the strand m.

$$p = \sqrt{j \frac{b}{b_c} \omega \mu_0 \sigma} = (1+j) \sqrt{\frac{b}{b_c} \frac{\omega \mu_0 \sigma}{2}} \quad (23)$$

$$p' = \sqrt{1-\varepsilon} p = (1+j) \sqrt{\frac{(1-\varepsilon)b}{b_c} \frac{\omega \mu_0 \sigma}{2}} \quad (24)$$

For the 150MW air-cooled turbo-generator, the upper and lower winding strands have different areas. For the numerical calculation, the boundary conditions of the electro-magnetic

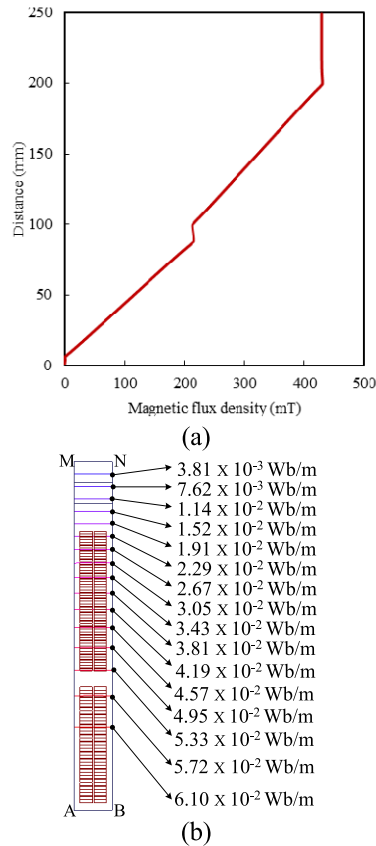


FIGURE 5. Flux distribution in the central of slot. (a) Magnetic flux density. (b) Magnetic line.

field equations could be written as

$$\begin{cases} \frac{\partial^2 A_z}{\partial x^2} + \frac{\partial^2 A_z}{\partial y^2} = j\mu_0\omega\sigma A_z - \mu_0 J_z \\ A_z|_{MN} = A_0 \\ \frac{\partial A_z}{\partial n} \Big|_{MA,AB,BN} = 0 \end{cases} \quad (25)$$

where A_z is magnetic vector potential, ω is the angular frequency, J_z is the strand current density, μ_0 is air relative permeability, σ is conductivity of the strand, and n is the normal unit vector.

The magnetic flux density and flux line are show in Fig. 5. Seen from Fig. 5, leakage magnetic flux density is relatively high at the top of slot and low at the bottom of slot. Due to the stator core permeability being considerably larger than that of the windings and insulation, the leakage magnetic flux crossing the slot is perpendicular to the two slot walls.

The eddy current consists of real and imaginary parts. The REC of strands (k_r) is equal to the ratio of resistance that is considered with the induced eddy current and resistance regarding no eddy current. Based on the magnetic

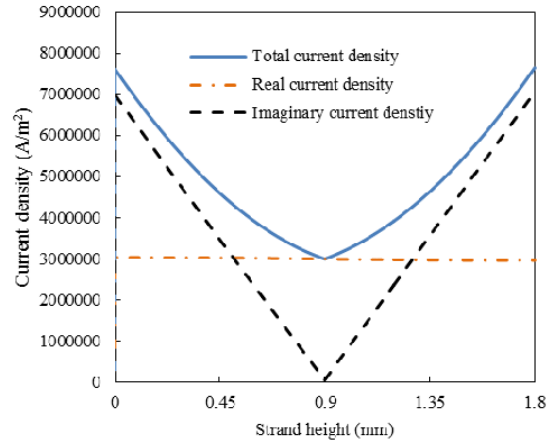


FIGURE 6. Eddy current density of the top strand in the upper winding.

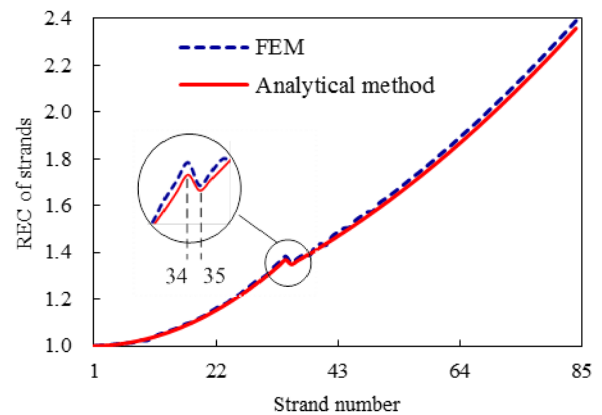


FIGURE 7. REC of strands.

filed solution, the REC could be expressed as

$$k_r = \frac{R_{ac}}{R_{dc}} = \frac{\iint_{S_b} |J_z|^2 dS}{J_{sz}^2 S_b} = \frac{\sum_{e=1}^n (J_{eR}^2 + J_{eI}^2) \Delta_e}{J_{sz}^2 S_b} \quad (26)$$

where R_{ac} is the resistance that is considered with the induced eddy current, R_{dc} is the resistance regarding no eddy current, J_z is the current density that contains the eddy current, J_{sz} is the source current density, J_{eR} and J_{eI} are the real and imaginary parts of the current density in element, S_b is the strand area, n is the total element number in one strand, and Δ_e is the element area.

The current density of real and imaginary parts of the top strand is shown in Fig. 6. The imaginary current density is lower in the center of the strand, and higher at the boundary of the strand. Fig. 7 shows the REC of strands from strands 1 to 84. The analytic and numerical calculation results of REC are matched. Due to the upper and lower winding strands that are not within the same area, the REC is not monotonically increasing from the bottom to the top of the slot. There is an inflection point from the top strand of the lower winding to the under strand of the upper winding.

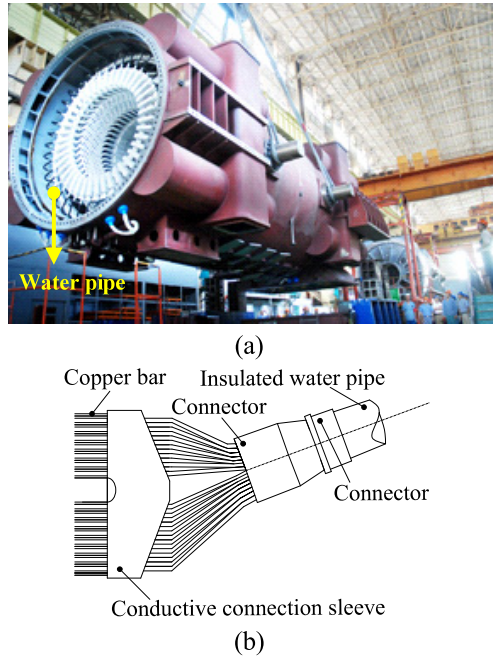


FIGURE 8. The stator structure of the 1000MW turbo-generator. (a) Prototype structure. (b) The connection of upper and lower windings.

TABLE 1. Rated parameters of the 1000MW generator.

Parameter under rated operation	Values
Power	1000 MW
Power factor	0.9
Stator voltage	27 kV
Stator current	23950 A
Frequency	50 Hz
Exciting voltage	660 V

III. THERMAL DISSIPATION IN LARGE POWER TURBO-GENERATOR BASED ON REC CALCULATION

For the 1000MW turbo-generator that is discussed in this paper, solid and hollow windings are adopted for the stator. The hollow strands are water-cooled. Fig. 8 gives the stator structure of this turbo-generator. The prototype structure is given in Fig. 8 (a). The upper winding and lower winding are connected by a conductive connection sleeve in the end part. The hollow strands are combined with water pipes by a connector. The connection type of upper and lower windings is shown in Fig. 8 (b).

The rated parameters are listed in Table 1. For the 1000MW power generator, there are 28 hollow strands in the upper winding, and 24 hollow strands in the lower winding. For the upper and lower winding strands, the solid and hollow strands are numbered from the bottom to the top as shown in Fig. 9 (a) and (b). Under rated operation, the calculated results of flux leakage and imaginary current density are shown in Fig. 9(c) and (d). It can be seen that the imaginary current density in the upper winding strands are obviously higher than those in the lower winding strands. For the hollow strands, their

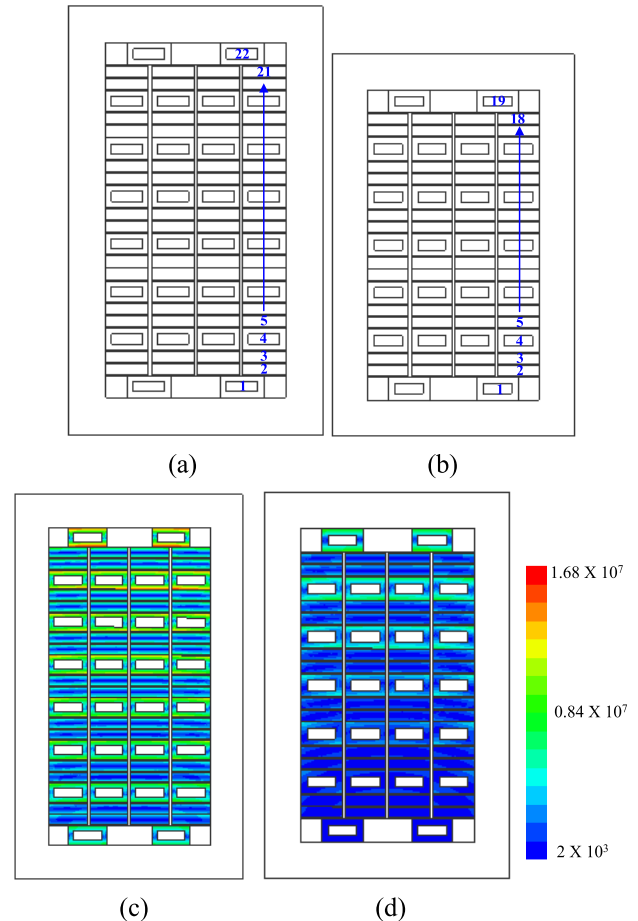


FIGURE 9. The strand number and current density. (a) Upper winding. (b) Lower winding. (c) Imaginary current density in up winding strands under rated operation (in A/m²). (d) Imaginary current density in down winding strands under rated operation (in A/m²).

imaginary current are obviously higher than those of the solid strands.

Fig. 10 gives the REC of the upper and lower windings. The RECs of the solid and hollow strands of the lower winding are lower than 1.5. The maximum REC of the hollow strands of the upper winding strand has exceeded 3.0.

According to the REC of the solid and hollow strands obtained by the calculation of the magnetic field, using the additional losses as the heat source, the thermal field of the turbo-generator stator strands is investigated. The temperature and fluid coupled model of the stator of 1000MW power turbo-generator is established. It is shown in Fig. 11 (a). The thermal and fluid coupled model consists of teeth, yoke, upper and lower windings, insulation, water pipes, hydrogen duct, and the slot wedge. The stator core is hydrogen-cooled, and the stator windings are water-cooled inside. There are 463,040 elements and 533,312 nodes in total in the solution region. The mesh plot of the thermal and fluid coupled model is shown in Fig. 11 (b) and (c).

The research on the flow and heat transfer process of the cooling medium involves the coupling analysis of temperature and fluid fields. During the calculation, the laws of

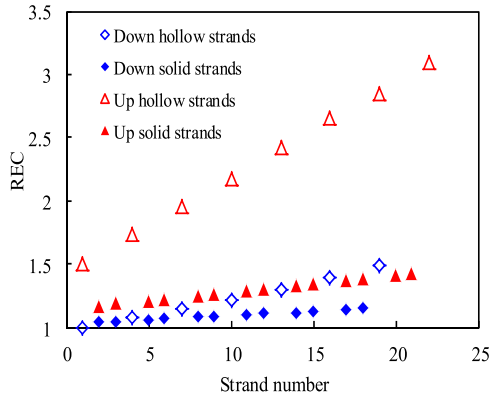


FIGURE 10. The REC of the upper and lower winding strands.

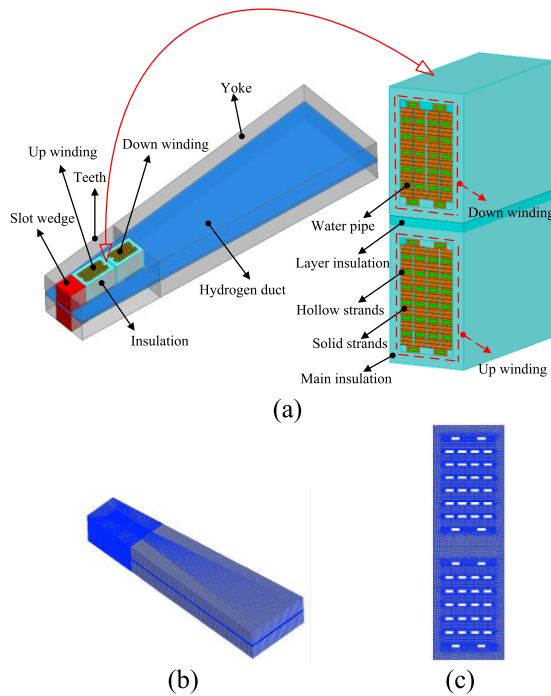


FIGURE 11. The stator thermal and fluid coupled model and its mesh plot. (a) The solution model. (b) Mesh plot of the solution region. (c) Mesh plot for one outer face of winding and its insulation except for water liquid.

conservation of mass, conservation of momentum, and conservation of energy should be satisfied. The calculation control equations for fluid-thermal coupling analysis are shown as follow [25].

$$\begin{cases} \frac{\partial \rho}{\partial t} + \text{div}(\rho \mathbf{u}) = 0 \\ \frac{\partial(\rho u)}{\partial t} + \text{div}(\rho \mathbf{u} u) = \text{div}(\mu \text{grad } u) - \frac{\partial P}{\partial x} + S_u \\ \frac{\partial(\rho v)}{\partial t} + \text{div}(\rho \mathbf{u} v) = \text{div}(\mu \text{grad } v) - \frac{\partial P}{\partial y} + S_v \\ \frac{\partial(\rho w)}{\partial t} + \text{div}(\rho \mathbf{u} w) = \text{div}(\mu \text{grad } w) - \frac{\partial P}{\partial z} + S_w \\ \frac{\partial(\rho T)}{\partial t} + \text{div}(\rho \mathbf{u} T) = \text{div}\left(\frac{\lambda}{c} \text{grad } T\right) + \frac{S_h}{c} \end{cases} \quad (27)$$

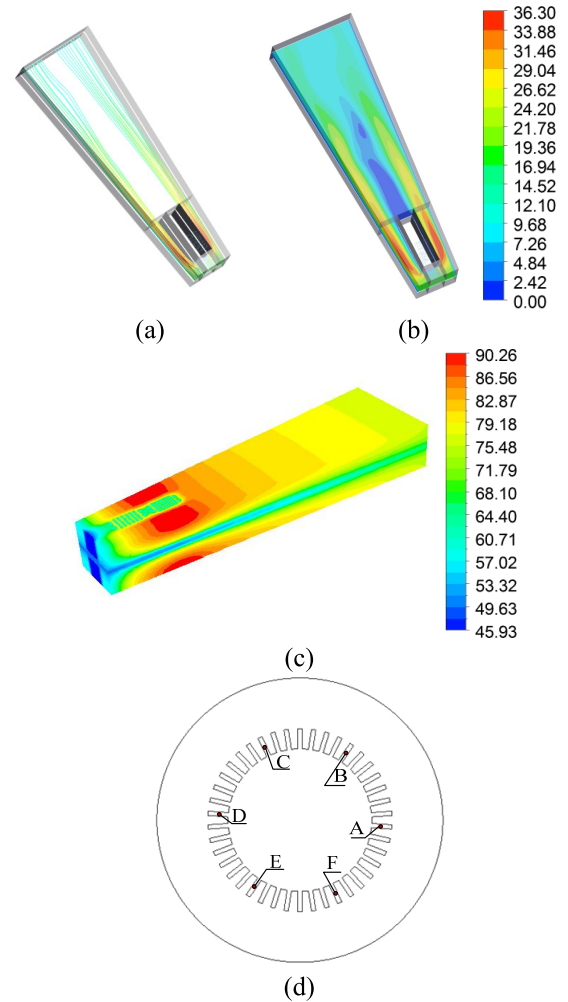


FIGURE 12. The path lines of hydrogen and velocity distribution in the ventilation duct and stator temperature distribution. (a) Stream lines. (b) Velocity distribution (in m/s). (c) The temperature distribution under rated operation (in °C). (d) The temperature sensors positions.

where ρ is the fluid density, t is the time, \mathbf{u} is the velocity vector, u, v, w are components of the x, y, z directions, μ is dynamic viscosity, P is fluid pressure, S_u, S_v, S_w are the general source term, S_h is the volumetric rate of heat generation, λ is thermal conductivity, c is specific heat, and T is temperature.

The 1000MW turbo-generator is water-hydrogen cooled. There is a ventilation duct between two stator core block. Fig. 12 (a) and (b) show the stream lines and velocity distribution in the hydrogen ventilation duct. It can be seen that the fluid velocity is high around the teeth, and lower around the yoke. The stator windings have a spoiler role on the hydrogen in the ventilation duct. The velocity is rather low at the bottom of the stator slot. The calculated results of the stator temperature of the rated operation condition is shown in Fig. 12 (c). The highest temperature is 90.3 °C, which appears on the stator teeth. Due to the windings are cooled by water, its temperature is not higher than that of the stator

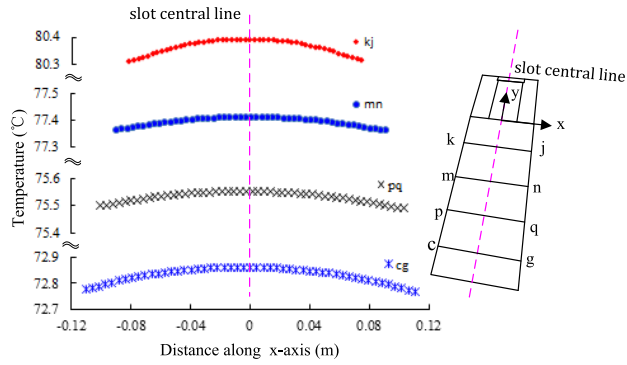


FIGURE 13. The temperature distribution on the yoke part (in °C).

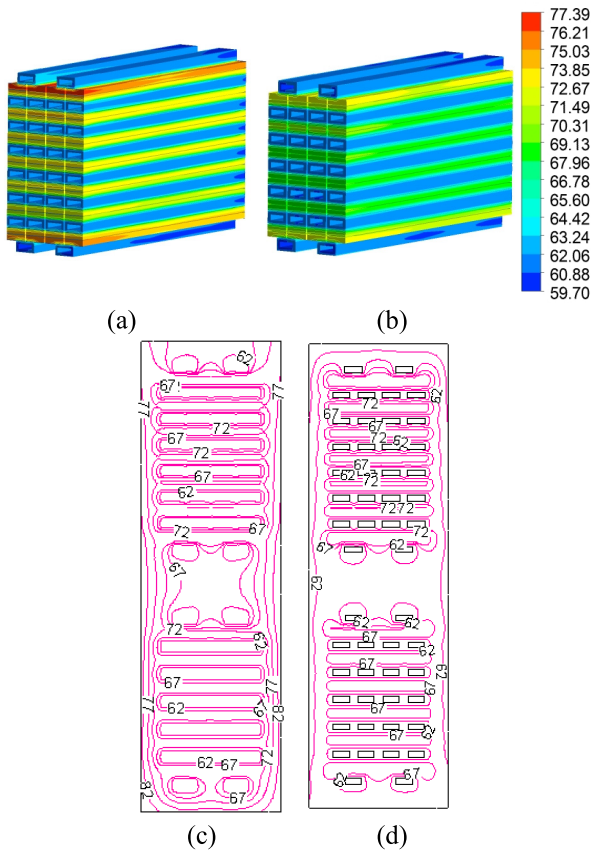


FIGURE 14. The temperature distribution on the upper and lower windings (in °C). (a) The upper one. (b) The lower one. (c) The position at the central of stator core inside. (d) The position at the central of ventilation duct inside.

teeth. The strand max. temperature is 77.4 °C that appears on the top solid strand. Fig. 12 (d) gives the thermal sensor position at the layer insulation of the stator winding. The thermal sensors, which are marked from #A to #F, are set and evenly distributed. Due to the fluid velocity being lower at the central part in the duct, the temperature of yoke is high at the extended position of slot central line than that of the two side as shown in Fig. 12(c). In order to illustrate the relationship, the temperature distribution on different trajectories of the yoke part is shown in Fig. 13.

TABLE 2. Comparison of calculated results with test data under rated load condition.

Structure	Test value(°C)	Calculated result(°C)
Layer insulation	#A	60.2
	#B	59.6
	#C	60.6
	#D	60.2
	#E	59.7
	#F	60.2
Outlet water temperature rise	19.1	17.2

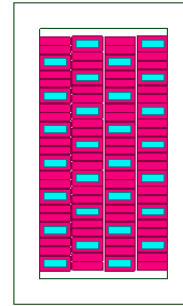


FIGURE 15. Staggered structure for solid and hollow strands.

In order to analyze the temperature distribution in the winding strands, Fig. 14 (a) and (b) give the temperature distribution of the upper and lower windings under rated operation condition.

Although the heat source of the hollow strands are higher than that of the solid strands due to the high eddy current density in the hollow strands, as the hollow strands are water-cooled, however their temperature are much lower than that of the solid ones. The winding temperature at the position of the stator core inside and the ventilation duct inside are shown in Fig. 14 (c) and (d).

To verify the solution results, the temperature in the layer insulation and the outlet of the water pipe were measured under rated load condition. The temperature testing method is the same as the one referenced in [21]. The comparison of the calculated and test results of the temperature are listed in Table 2. The calculated temperature results of the 1000MW generator that is considered the strand’s REC well match the test data.

In order to reduce the REC, a new winding configuration shown in Fig. 15 is discussed. Different from the original structure, the new structure of the winding is with the hollow and solid strands being staggered. For the new assemblies, the maximum REC of the upper solid strand is 1.37, which is 1.42 for the original structures. The maximum REC of the upper hollow strand is 3.03, which is 3.1 for the original structures. The average REC of the up strands is 1.567, which is 1.672 for the original structures. The average REC of the down strands is 1.085, which is 1.167 for the original structures. Compared with the original structure, the winding temperature could be reduced by 1.6 °C with staggered structure for solid and hollow strands.

It can be seen that the REC is reduced by adopting the staggered structure. However, the slot construction and the dimension of each strand are not changed, which doesn't increase the manufacturing cost of the generator.

IV. CONCLUSION

1. For large turbo-generators, due to the stator upper and lower windings with different structures, the REC does not monotonically increase from the bottom to the top of the slot. There is an inflection point from the top strand of the lower winding to the bottom strand of the upper winding.

2. The average additional winding loss of the upper one is seven times that in the lower one when their total areas are the same. The average REC is directly proportion to the total height and strand area, and is inversely proportional to the slot width. It is irrelevant to the winding current value.

3. The 1000MW power turbo-generator windings are water-cooled from the inside, which results in the winding temperature being lower in the stator part. The maximum temperature appears on the stator teeth.

4. Due to the high eddy current density in the hollow strands, the heat source of the hollow strands are higher than that of the solid strands. Meanwhile, as the hollow strands are water-cooled, the temperature of the hollow strands are much lower than that of the solid ones.

REFERENCES

- [1] P. Arumugam, T. Hamiti, C. Brunson, and C. Gerada, "Analysis of vertical strip wound fault-tolerant permanent magnet synchronous machines," *IEEE Trans. Ind. Electron.*, vol. 61, no. 3, pp. 1158–1168, Mar. 2014.
- [2] H. Hamalainen, J. Pyrhonen, J. Nerg, and J. Talvitie, "AC resistance factor of litz-wire windings used in low-voltage high-power generators," *IEEE Trans. Ind. Electron.*, vol. 61, no. 2, pp. 693–700, Feb. 2014.
- [3] M. van der Geest, H. Polinder, J. A. Ferreira, and D. Zeilstra, "Current sharing analysis of parallel strands in low-voltage high-speed machines," *IEEE Trans. Ind. Electron.*, vol. 61, no. 6, pp. 3064–3070, Jun. 2014.
- [4] D. A. Gonzalez and D. M. Saban, "Study of the copper losses in a high-speed permanent-magnet machine with form-wound windings," *IEEE Trans. Ind. Electron.*, vol. 61, no. 6, pp. 3038–3045, Jun. 2014.
- [5] K. Zhou and L. Cai, "Online measuring power factor in AC resistance spot welding," *IEEE Trans. Ind. Electron.*, vol. 61, no. 1, pp. 575–582, Jan. 2014.
- [6] F. J. T. E. Ferreira, M. V. Cistelecan, and A. T. de Almeida, "Comparison of different tapped windings for flux adjustment in induction motors," *IEEE Trans. Energy Convers.*, vol. 29, no. 2, pp. 375–391, Jun. 2014.
- [7] F. Xiong and X. Wang, "Design of a low-harmonic-content wound rotor for the brushless doubly fed generator," *IEEE Trans. Energy Convers.*, vol. 29, no. 1, pp. 158–168, Mar. 2014.
- [8] C. R. Sullivan, "Optimal choice for number of strands in a litz-wire transformer winding," *IEEE Trans. Power Electron.*, vol. 14, no. 2, pp. 283–291, Mar. 1999.
- [9] X. Nan and C. R. Sullivan, "An equivalent complex permeability model for litz-wire windings," *IEEE Trans. Ind. Appl.*, vol. 45, no. 2, pp. 854–860, Mar./Apr. 2009.
- [10] S. Iwasaki, R. Deodhar, Y. Liu, A. Pride, Z. Q. Zhu, and J. Bremner, "Influence of PWM on the proximity loss in permanent magnet brushless AC machines," in *Proc. IEEE Ind. Appl. Soc. Annu. Meeting*, Oct. 2008, pp. 1359–1367.
- [11] J. Islam, J. Pippuri, J. Perho, and A. Arkkio, "Time-harmonic finite-element analysis of eddy currents in the form-wound stator winding of a cage induction motor," *IET Electr. Power Appl.*, vol. 1, no. 5, pp. 839–846, Sep. 2007.
- [12] G. J. Atkinson, B. C. Mecrow, A. G. Jack, D. J. Atkinson, P. Sangha, and M. Benarous, "The analysis of losses in high-power fault-tolerant machines for aerospace applications," *IEEE Trans. Ind. Appl.*, vol. 42, no. 5, pp. 1162–1170, Sep. 2006.
- [13] J.-R. Sibue, J.-P. Ferrieux, G. Meunier, and R. Periot, "Modeling of losses and current density distribution in conductors of a large air-gap transformer using homogenization and 3-D FEM," *IEEE Trans. Magn.*, vol. 48, no. 2, pp. 763–766, Feb. 2012.
- [14] R. Wrobel, A. Mlot, and P. H. Mellor, "Contribution of end-winding proximity losses to temperature variation in electromagnetic devices," *IEEE Trans. Ind. Electron.*, vol. 59, no. 2, pp. 848–857, Feb. 2012.
- [15] C. R. Sullivan, "Computationally efficient winding loss calculation with multiple windings, arbitrary waveforms, and two-dimensional or three-dimensional field geometry," *IEEE Trans. Power Electron.*, vol. 16, no. 1, pp. 142–150, Jan. 2001.
- [16] J. Acero, P. J. Hernandez, J. M. Burdio, R. Alonso, and L. A. Barragan, "Simple resistance calculation in litz-wire planar windings for induction cooking appliances," *IEEE Trans. Magn.*, vol. 41, no. 4, pp. 1280–1288, Apr. 2005.
- [17] Z. Kolondzovski, A. Belahcen, and A. Arkkio, "Comparative thermal analysis of different rotor types for a high-speed permanent-magnet electrical machine," *IET Electr. Power Appl.*, vol. 3, no. 4, p. 279, 2009.
- [18] P. Sergeant, D. Hectors, L. Dupré, and K. Van Reusel, "Thermal analysis of magnetic shields for induction heating," *IET Electr. Power Appl.*, vol. 3, no. 6, p. 543, 2009.
- [19] G. J. Li, J. Ojeda, E. Hoang, and M. Gabsi, "Thermal-electromagnetic analysis of a fault-tolerant dual-star flux-switching permanent magnet motor for critical applications," *IET Electr. Power Appl.*, vol. 5, no. 6, p. 503, 2011.
- [20] Y. Fan, X. Wen, and S. A. K. S. Jafri, "3D transient temperature field analysis of the stator of a hydro-generator under the sudden short-circuit condition," *IET Electr. Power Appl.*, vol. 6, no. 3, p. 143, 2012.
- [21] P. L. Dowell, "Effects of eddy currents in transformer windings," *Proc. Inst. Electr. Eng.*, vol. 113, no. 8, p. 1387, 1966.
- [22] J. A. Ferreira, "Improved analytical modeling of conductive losses in magnetic components," *IEEE Trans. Power Electron.*, vol. 9, no. 1, pp. 127–131, Jan. 1994.
- [23] R. P. Wojda and M. K. Kazimierczuk, "Analytical optimization of Solid-Round-wire windings," *IEEE Trans. Ind. Electron.*, vol. 60, no. 3, pp. 1033–1041, Mar. 2013.
- [24] J. Acero, R. Alonso, J. M. Burdio, L. A. Barragan, and D. Puyal, "Frequency-dependent resistance in litz-wire planar windings for domestic induction heating appliances," *IEEE Trans. Power Electron.*, vol. 21, no. 4, pp. 856–866, Jul. 2006.
- [25] H. K. Versteeg and W. Malalasekera, *An Introduction to Computational Fluid Dynamics: The Finite Volume Method*. Upper Saddle River, NJ, USA: Prentice-Hall, 2007, pp. 72–78.



LIKUN WANG (Member, IEEE) received the B.E., M.E., and D.E. degrees in electrical machinery and appliance from the Harbin University of Science and Technology (HUST), Harbin, China, in 2010, 2013, and 2015, respectively. Since 2017, he has been a Postdoctoral Fellow with the Institute of Electromagnetic and Electronic Technology, Harbin Institute of Technology. Since 2018, he has been an Associate Professor with the College of Electrical and Electronic Engineering,

HUST. His research interest includes synthesis physical fields and dynamic operation mechanism of electrical machines and its systems. He received the Second Prize from the Science and Technology Progress of Heilongjiang Province, in 2019.



motors and linear electromagnetic drives, control of the power quality, and superconducting motors.

BAOQUAN KOU (Member, IEEE) received the B.E. degree from the Harbin Institute of Technology (HIT), China, in 1992, the M.E. degree from the Chiba Institute of Technology, Japan, in 1995, and the D.E. degree from HIT, in 2004. From 2005 to 2007, he held a postdoctoral position with Mobile Station, HIT. Since 2007, he has been a Professor with the School of Electrical Engineering and Automation, HIT. His research interests include electric drive of electric vehicles, linear



dozens of articles with the IEEE TRANSACTIONS and other technical and scientific journals. He has taken charge of the National Science and Technology Support Project, the Key Project in the National Science and Technology Pillar Program, the National Key Research and Development Program, and so on. He specializes in new energy transportation and motor drive.

WEI CAI received the B.E. and M.E. degrees in electrical engineering from the Harbin University of Science and Technology (HUST), in 1982 and 1985, respectively, and the D.E. degree in electrical and computer engineering from Clarkson University, Potsdam, NY, USA, in 1999. Since 2019, he has been a Professor with the College of Electrical and Electronic Engineering, HUST. He was selected as an Expert of the National Thousand Talents Plan, in 2010. He has published

• • •